RSC Advances

PAPER

View Article Online
View Journal | View Issue

Cite this: *RSC Adv.*, 2015, **5**, 61161

Adsorption behavior of a computer-aid designed magnetic molecularly imprinted polymer *via* response surface methodology†

Kai Zhang,[a] Wenyue Zou,[a] Hongyan Zhao,[ab] Pierre Dramou,[a] Chuong Pham-Huy,[c] Jia He[a] and Hua He*[ad]

A novel magnetic molecularly imprinted polymer (MMIP) has been designed using flexible docking and molecular dynamics in computer simulation. Six kinds of representative functional monomers have been screened to obtain the optimal one, as well as optimizing its ratio to the template amlodipine (AML). Two MMIPs have been prepared with the most suitable functional monomer methacrylic acid (MAA) along with acrylamide (AM) as a comparison, in the ratio of 4 to AML. Fourier transform infrared (FT-IR) spectroscopy, transmission electron microscopy (TEM), scanning electron microscopy (SEM), and vibrating sample magnetometery (VSM) were used to characterize the structure, morphology and magnetic properties of the MMIPs. A static adsorption study was carried out with the help of response surface methodology (RSM) and in addition, adsorption kinetics and isotherms were studied to further explain the adsorption behavior. Three dihydropyridine calcium channel blockers (DHP-CCBs) as structural analogues and non-structural analogue penicillin V potassium were chosen for the selectivity study. The results showed that MMIP using MAA as functional monomer had a large adsorption capacity (53.77 μg mg^{-1}) as well as a large imprinting factor (more than 2) and the adsorption behavior was in accordance with a pseudo-second-order model and Freundlich isotherm model. Due to the excellent properties of the polymer: good magnetic properties, large adsorption capacity and great selectivity for DHP-CCBs, a magnetic molecularly imprinted solid phase extraction with ultraviolet detection (M-MISPE-UV) method had been established, validated and applied to the analysis of AML in urine sample.

Received 1st June 2015
Accepted 9th July 2015

DOI: 10.1039/c5ra10367c

www.rsc.org/advances

Introduction

A molecularly imprinted polymer (MIP) is an environmentally friendly and recyclable material with characteristics of high selectivity and strong anti-interference ability to be widely implemented in various types of sensors,[1] adsorbents for solid phase extraction[2] and drug delivery systems.[3] With magnetic separation, magnetic molecularly imprinted polymers (MMIP) have overcome the shortage of traditional MIPs which is that it is time-consuming to separate them from the matrix through centrifugation or filtration.[4–6]

Molecularly imprinted polymers synthesized by various functional monomers, cross-linkers and solvents have been extensively studied in recent decades. However, the methods of design, synthesis and performance evaluation of MIP are still mainly relying on tedious trials and errors or reported methods. To satisfy the requirements of modern research, a fast, accurate, and economical method to screen the constituents of MIPs is of great significance. For rational design and selecting a suitable synthesis method for MIP, a growing number of research groups have focused on computer simulation and computer-aided design.[7–10] Screening the constitution of MIP by computer simulation can be traced back to 1999, the group of Sergeyeva[11] introduced a method to design atrazine MIP with methacrylic acid (MAA) as functional monomer in HyperChem 3.0 and found that atrazine and MAA have formed strong interaction by two ionic and three hydrogen bonds. Since then, more and more accurate algorithms and models from molecular mechanics, quantum mechanics, and Monte Carlo method to molecular dynamics[8] have been designed and applied in the design of MIP with the development of quantum chemistry and computer science. With various softwares such as PRODRUG SERVER,[12] Gaussian[13,14] and Discovery studio,[15] researchers have concentrated on simulating the real conditions of reaction as possible. Different simulation methods have been established for

[a]*Department of Analytical Chemistry, School of Sciences, China Pharmaceutical University, Nanjing 210009, Jiangsu, China. E-mail: jcb_321@163.com; dochehua@163.com*

[b]*Department of Hygienic Analysis and Detection, School of Public Health, Nanjing Medical University, Nanjing, Jiangsu 211166, China*

[c]*Faculty of Pharmacy, University of Paris V, Paris, 75006 France*

[d]*Key Laboratory of Drug Quality Control and Pharmacovigilance, Ministry of Education, China Pharmaceutical University, Nanjing 210009, China*

† Electronic supplementary information (ESI) available. See DOI: 10.1039/c5ra10367c

selection of functional monomer as well as solvent, and further study on the molecular recognition mechanism.

Selectivity and adsorption capacity are the most important evaluation indicators for MIP. An excellent molecularly imprinted material should have special selectivity for the template as well as its structural analogues and a large adsorption capacity should be guaranteed at the same time to meet the requirements of different application. However, adsorption behavior of MIP is influenced by manifold factors greatly. In order to obtain the optimum adsorption conditions rapidly and accurately, multiple factor experiments will take plenty of time and costs, while orthogonal experimental design can only screen several certain combinations to obtain a better value instead of the best within the given range of conditions.[16] Response surface methodology (RSM) is an experimental design and optimization method in production engineering,[17–19] through a series of certainty test fitting a response surface to simulate the real state surface. To establish an appropriate mathematical model, only few experiments will be done to achieve multiple linear regression and the optimal conditions can be fund intuitively through the response surface.

Amlodipine as a dihydropyridine calcium channel blocker is the first line drug in the treatment of different hypertensions.[20] Because of the serious side effects of *R*-(+)-amlodipine such as peripheral edema, fatigue and dizziness, major active ingredient *S*-(−)-amlodipine (AML) has gradually replaced the racemate in clinical treatment.[21] AML is well absorbed by oral administration and renal elimination is the major route of excretion with about 60% of administered dose recovered in urine. To detect AML in biological samples, solid-phase extraction (SPE) is routinely needed before analysis to eliminate the interference of matrix.

In this work, a novel magnetic molecularly imprinted polymer for amlodipine was prepared by precipitation method coupled with a computer simulation approach and the adsorption behavior of the material was studied by adsorption statics with the help of response surface methodology, and adsorption kinetics, isotherm and selectivity. We successfully combined flexible docking and molecular dynamics method in computer simulation to screen the most suitable functional monomer and its ratio to AML for magnetic molecularly imprinted polymer and using the response surface methodology in the optimization of adsorption process. A magnetic molecularly imprinted solid phase extraction with ultraviolet detection (M-MISPE-UV) method has been established and validated for the detection of amlodipine in human urine sample.

Experimental

Materials

AML, felodipine (FEL), and nimodipine (NIM) were purchased from Hubei Xing Galaxy Chemical Co., Ltd (Wuhan, China), nifedipine (NIF) and penicillin V potassium (PENI) from National Institutes for Food and Drug Control (Beijing, China). Ferric chloride hexahydrate (Fe^{3+}), dimethyl sulfoxide (DMSO) and polyvinylpyrrolidone (PVP) were purchased from Sinopharm Chemical Reagent Co., Ltd (Shanghai, China). Ferrous sulfate heptahydrate (Fe^{2+}), ammonium hydroxide ($NH_3 \cdot H_2O$) and acetic acid were obtained from Nanjing Chemical Reagent Co., Ltd (Nanjing, China). Ethylene glycol dimethacrylate (EGDMA) and methacrylic acid (MAA) were obtained from Aladdin Industrial Corporation (Shanghai, China). Methanol and acrylamide (AM) were purchased from Jiangsu Hanbon Sci. &Tech. Co., Ltd (Huaian, China) and Nanjing Sangon Biotech Co., Ltd (Nanjing, China), respectively. All these chemicals and solutions used were of analytical reagent grade.

Instruments and softwares

UV-visible spectrophotometer (UV-1800) and Fourier-transform infrared spectrophotometer (FT-IR-8400S) were purchased from Shimadzu (Kyoto, Japan). An S-3000 scanning electron microscopy (SEM, Hitachi Corporation, Japan) and an FEI Tecnai G2 F20 transmission electron microscope (TEM) were used to characterize the morphology of the materials. The magnetic properties were tested by a LDJ 9600-1 vibrating sample magnetometer (VSM) operating at room temperature with applied fields up to 10 kOe. Computer simulation was carried out *via* Molecular Operating Environment (MOE, v2008) and Discovery Studio (DS, v2.5). Design-Expert (v8.0) was used in response surface methodology.

Computer simulation

The template AML and six representative functional monomers MAA, acrylic acid (AA), methacrylamide (MAM), AM, 2-vinylpyridine (2-VP), 4-vinylpyridine (4-VP) were constructed and preliminary optimization at a gradient of 0.1 in MOE. Steepest descent and conjugate gradient method in minimization module were applied 1000 steps respectively to obtain the minimal energies of each 3D structure in DS. A flexible docking programme CDOCKER was used to simulate the interaction between AML and the functional monomers with the ratio from 1 : 1 to 1 : 6 in the complex force field of CHARMm and MMFF94 in DS. The docking energy can be calculated by the following formula:[7]

$$\Delta E = |E_{\text{complex}} - E_{\text{template}} - E_{\text{monomer}}| \quad (1)$$

where ΔE is the docking energy, E_{complex} represents the energy of the template–monomer complex, E_{template} and E_{monomer} represent the energies of the template and functional monomer respectively.

Molecular dynamics simulation was conducted by dynamics (equilibration) method from the simulation module in DS to study the evolution of motion state of all complexes. Potential energy, kinetic energy, and equilibrium temperature were calculated as well as the numbers of the hydrogen bonds counted to evaluate the balance and interaction of the complexes.

Synthesis and characterization of magnetic polymers

The iron core Fe_3O_4 was prepared by a chemical precipitation method according our previous study.[14] Briefly, the solution of 0.02 mmol Fe^{2+} and 0.04 mmol Fe^{3+} were heated to 80 °C under the nitrogen gas protection. Ammonium hydroxide was added

dropwise until the pH was between 10 and 11. With vigorous mechanical stirring for 2 hours, the precipitate was collected and wash by distilled water and dried in vacuum. The MMIPs were prepared as follow: AML (0.5 mmol) and MAA or AM (2 mmol) were dissolved in 5 mL DMSO while 0.5 g Fe_3O_4 in 2.5 mL DMSO under ultrasound for 10 min. Then, the EGDMA (10 mmol) was mixed with the above-mentioned solutions. PVP (0.2 g) in 50 mL of DMSO–H_2O (9 : 1, v/v) was heated to 60 °C under the nitrogen gas protection and vigorous mechanical stirring, and the mixture was transferred to the three-necked round bottomed flask. AIBN (0.05 g) was added and the reaction was maintained for 10 h. The polymers were separated and washed by distilled water and methanol–acetic acid (8 : 2, v/v) several times until the washing solution could not be detected at 364 nm by UV-1800 in the range of 190 to 400 nm. Finally, MMIPs using MAA or AM as functional monomer (MAA-MMIP or AM-MMIP) were dried in vacuum. The synthesis of two corresponding magnetic non-imprinted polymers (MAA-MNIP and AM-MNIP) were operated without adding AML. Morphology characteristics of magnetic polymers were obtained by SEM and TEM while structure information by infrared spectrum. To test the magnetic property of MMIPs, a magnet was placed around the bottle with 50 mg MAA-MMIP in aqueous solution and VSM for further specific magnetic characteristic.

Optimization of adsorption conditions with response surface methodology

According to Box–Behnken Design (BBD),[16,22] amount of materials (5, 10, 15 mg), concentration of solution (25, 50, 75 μg mL^{-1}) and incubating temperature (298, 310.5, 323 K) three main factors affecting the adsorption behavior in three levels were chose and 17 combination were experimented. The equilibrium adsorption capacity (Q, μg mg^{-1}) of AML bound to the material is calculated by the following formula:

$$Q = (C_0 - C_1) \times V/m \quad (2)$$

where C_0, C_1, V and m represent the initial concentration of AML (μg mL^{-1}), the equilibrium concentration in the supernatant (μg mL^{-1}), the volume of the solution (mL) and the amount of the polymer (mg), respectively. Relevant model was established and validated using the tested data in Design-Expert. Response surface was obtained to figure out the optimal conditions so the maximum value of equilibrium adsorption capacity (Q_{max}) within the prescribed range was predicted and verified by actual trials.

Binding property study

Adsorption kinetics study was investigated by the adsorption amount of 25 mg MAA-MMIP or AM-MMIP in 50 mL 75 μg mL^{-1} AML solution in different time intervals (0–180 min). Adsorption isotherm study was investigated by the adsorption amount of 5 mg MAA-MMIP or AM-MMIP in 10 mL AML solution in different initial concentration (25–75 μg mL^{-1}). After 2 h incubating at 25 °C with shaking, the materials were separated by a magnet and the unbound AML in the supernatant was measured by UV-1800 scanning from 190 to 400 nm.

Selectivity study and determination of AML in urine sample

10 mL AML, NIM, NIF, FEL or PENI solution with standard concentration of 75 μg mL^{-1} was added into 5 mg four different materials respectively. After incubating 2 h at 25 °C with shaking, separated by a magnet and detected by UV-1800. The selectivity of MMIPs can be evaluated[5,23] by imprinting factor (α) and selectivity factor (β):

$$\alpha = Q_{MMIP}/Q_{MNIP} \quad (3)$$

$$\beta = \alpha_1/\alpha_2 \quad (4)$$

where Q_{MMIP} and Q_{MNIP} represent the adsorption amount (μg mg^{-1}) of MMIP and MNIP to AML respectively. α_1 and α_2 represent the imprinting factor of the polymer to AML or other analytes. Non-treated human urine was spiked with AML to the concentration of 5, 25, 75 μg mL^{-1} respectively. 5 mg MAA-MMIP was added into 10 mL above-mentioned solutions respectively. Loading and elution processes were carried out as follow: after incubating for 2 h in room temperature, the polymer was separated by magnet and washed by 2 mL eluent which is constitute of methanol–acetic acid (8 : 2, v/v) twice. Dried the eluent, redissolved in 3 mL distilled water and detected by UV-1800.

Results and discussion

Computer simulation

A strong interaction between template and functional monomer is the guarantee of molecular recognition.[24] Most widely used functional monomers including carboxylic acids (MAA, AA), acidamides (MAM, AM) and heterocyclic base (2-VP, 4-VP) were screened. Optimized 3D structures of template AML and six functional monomers were obtained from MOE and further energy optimization was conducted in DS. Steepest descent method in minimization module was used to decrease the system energy towards the negative direction until the energy remained constant. In the proximity of the point of minimum energy, conjugate gradient method was used to achieve rapid convergence. The energy value of each compound was calculated[25] (see S1†). The optimized 3D structures became the initial conformation for flexible docking. Using simulated annealing algorithm, CDOCKER programme in receptor–ligand interactions module set AML as receptor and function monomer as ligand. The most appropriate docking pose was chose from ten possible positions determined by scoring function (-CDOCKER_ENERGY). Docking energies in Fig. 1A showed great difference among complexes formed by template AML and six functional monomers with different ratio. Docking energy of AML and 4 MAA (24.95 kcal mol^{-1}) was larger than other complexes and the higher docking energy indicates that the functional monomer and template formed a more stable complex with a strong interaction.[9] The biggest docking energy of AML and other functional monomers (AA, MAM, AM, 2VP, 4VP) were 16.51, 18.78, 18.97, 16.25, and 15.03 kcal mol^{-1} in the ratio of 1 : 2, 1 : 6, 1 : 4, 1 : 2 and 1 : 5 respectively (see S2†). The best ratio of AML to MAA and AM is 1 : 4, therefore, molecular dynamics simulation was conducted to study the

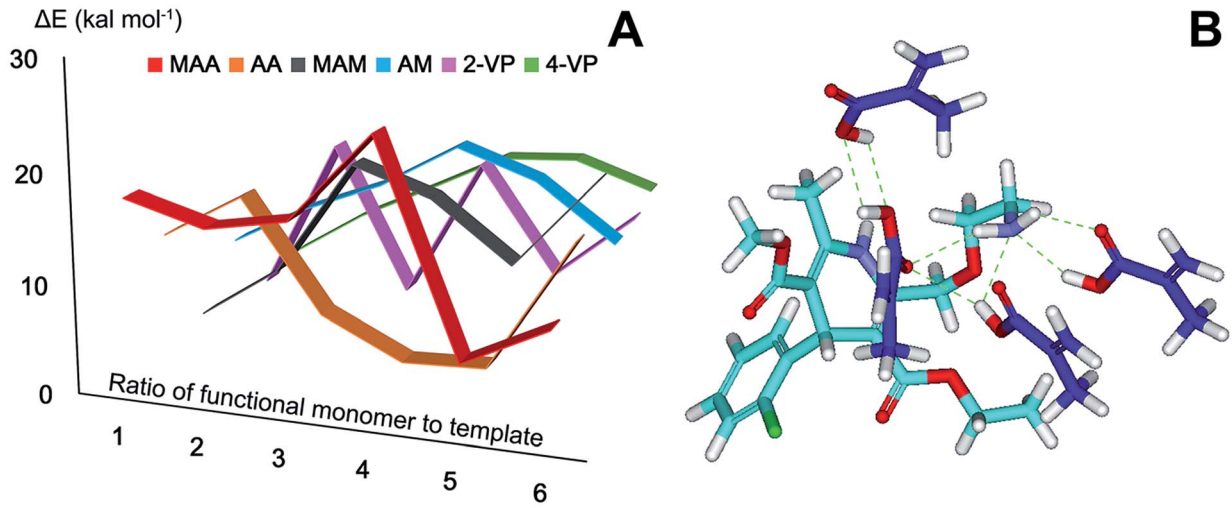

Fig. 1 (A) Docking energies of template with 6 functional monomers; (B) the optimal combination position of template and MAA (mol ratio of 1 : 4).

interaction with time of the two complexes and the main combination ways. Potential energy, kinetic energy, equilibrium temperature and the number of the hydrogen bonds listed in Table 1 illustrated the form and strength of interaction for of each complex. In MAA–AML complex, there were 7 hydrogen bonds formed as showed in Fig. 1B while only 3 in AM–AML complex. In molecular weak interactions, hydrogen bond is the strongest interaction in all kinds of secondary bonds and especially for MIP prepared by non-covalent approach, hydrogen bonds are the main force in the formation of selective recognition sites as well as in the process of molecular recognition.[26]

MAA is a common functional monomer as a hydrogen bond acceptor as well as a receptor so it is suitable for the templates that have hydrogen bonding interaction sites as AML.[27] The potential energy of MAA–AML complex was −69.73 kcal mol^{-1} which is much larger than that of AM–AML complex implying that the interaction of AML and MAA was stronger than AML and AM. The final dynamic equilibrium state of MAA–AML complex was in the condition of 299.49 K which was near to the room temperature and it was the reason why the complex had a higher kinetic energy compared with AM–AML complex. The consistent results in flexible docking and molecular dynamics simulation show that MAA is the most suitable functional monomer to prepare MIP. Hence both MAA-MMIP and AM-MMIP were prepared to verify the results of computer simulation and explore the difference in selectivity and adsorption capacity of the polymers.

Table 1 Dynamics equilibrium parameters

Complexes	Hydrogen bonds	Potential energy (kcal mol^{-1})	Kinetic energy (kcal mol^{-1})	Temperature (K)
MAA–AML	7	−69.73	88.38	299.49
AM–AML	3	−120.24	78.70	290.14

Synthesis of MMIP

In order to verify the accuracy of computer simulation, MAA-MMIP, AM-MMIP and two non-imprinted polymers (MAA-MNIP, AM-MNIP) as comparison have been prepared. The added amount of Fe_3O_4, the ratio of template, functional monomer and cross-linker, porogen and solvent were chose according to our previous works.[14,28] To acquire a MMIP with high selectivity and adsorption capability, the polymerization time and temperature were set at 10 h and 60 °C, the eluent to remove AML and other unreacted reagents in MMIPs was methanol–acetic acid (8 : 2, v/v) while distilled water and methanol for MNIPs to avoid structural damage.

Characterizations

The scales of TEM images for MAA-MMIP in Fig. 2A were 100 nm and 20 nm, indicating the polymer to be in the range of

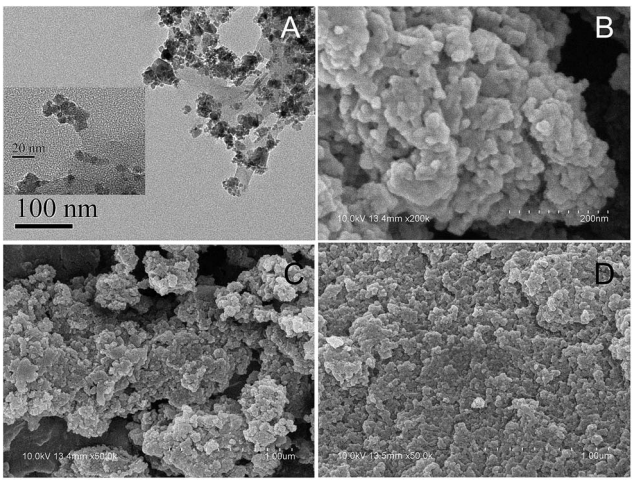

Fig. 2 TEM images (A) for MAA-MMIP and SEM images for MAA-MMIP (B, C) and AM-MMIP (D). Scale bar: 20 nm and 100 nm for (A); 200 nm for (B); and 1 μm for (C) and (D).

nanometer and formed spherical beads by precipitation polymerization method. The SEM images of MAA-MMIP (Fig. 2B and C) and AM-MMIP (Fig. 2D) illustrated the significantly different morphologies of MMIPs prepared by different functional monomers. At the same scale of 1 μm, a large number of cavities can be found for MAA-MMIP while compared with AM-MMIP, a flat surface had a huge impact on the behavior of adsorption and release and resulted in the low adsorption capability.

In addition, porous structure of MAA-MMIP can also accelerate the process of mass transfer and significantly shorten the required time for adsorption and elution equilibrium.[29] MAA-MMIP with better features of morphology showed that the functional monomer selected by computer simulation was suitable in the preparation of the MMIP.

The magnetic saturation (M_s) value of Fe_3O_4 is 49.13 emu g^{-1} in VSM test while MAA-MMIP and AM-MMIP are 16.58, 14.67 emu g^{-1}. The decrease of M_s value is the evidence of molecularly imprinted polymer layer coated on the iron core.[14] As showed in Fig. 3A, the magnetic polymer was separated rapidly under the condition of external magnet ensuring the application of the material in aqueous environment.

The infrared spectra of Fe_3O_4, MMIPs and MNIPs in Fig. 3B show the main structure of five nanoparticles. The same peaks: 582, 1132, 1432 cm^{-1} were the existence of Fe_3O_4 core indicating the structure of Fe_3O_4 remain unchanged in the polymerization.[30] Other common peaks as 3437, 2949, 1717 cm^{-1} due to the stretching vibration of the O–H, C–H and C=O bond belong to the carboxyl and amide group in MAA and AM respectively. All the information in infrared spectra show that the polymers have been successfully prepared.

Optimization of adsorption behavior with response surface methodology

To optimize the adsorption behavior of MAA-MMIP to AML in aqueous environment, three main factors influencing the adsorption behavior in three levels have been considered and 17 experiments had been carried out to build the model according to BBD[16] (see S3†). *A*, *B* and *C* represent the amount of polymers (mg), concentration of solutions (μg mL^{-1}) and temperature (K) respectively. *C* was set as ordinal factor in high ($C[1] = 1$, $C[2] = 1$), middle ($C[0] = 0$, $C[2] = -2$), and low ($C[-1] = 1$, $C[2] = 1$) adsorption temperature while *A* and *B* as continuous.

Table 2 Analysis of variance for response surface quadratic model

Source	Sum of squares	Df[d]	Mean square	*F* value	*p*-value
Model	1355.38	11	123.22	6459.89	<0.0001
A^a	557.95	1	557.95	29 251.70	<0.0001
B^b	608.13	1	608.13	31 882.81	<0.0001
C^c	116.51	2	58.25	3054.15	<0.0001
AB	1.73	1	1.73	90.66	0.0002
AC	25.32	2	12.66	663.68	<0.0001
BC	16.82	2	8.41	440.83	<0.0001
A^2	0.085	1	0.085	4.44	0.0891
B^2	29.16	1	29.16	1528.92	<0.0001
Residual	0.095	5	0.019		
Lack of fit	0.048	1	0.048	4.06	0.1141
Pure error	0.047	4	0.012		

[a] Amount of polymer (mg). [b] Concentration of solutions (μg mL^{-1}). [c] Temperature (K). [d] Degree of freedom.

Response surface quadratic model has been chose with the high *R*-squared coefficient (0.9999) and adjusted *R*-squared coefficient (0.9998) and the low coefficient of variation for the model (0.48%) (see S4†). Datas for analysis of variance[17] are listed in Table 2.

The model *F*-value of 6459.89 implies the model is significant and there is only a 0.01% chance that a "Model *F*-Value" this large could occur due to noise.[31] Values of "*p*-value" less than 0.05 indicate model terms are significant. In this case, only one model term A^2 is not significant which the demand of the hierarchy for quadratic model. *F* value of 0.048 in lack of fit test implies model value is not significant relative to the pure error and the *p* value of 0.1141 is large than set point (0.05) that indicates the model fits the experiment datas well and no

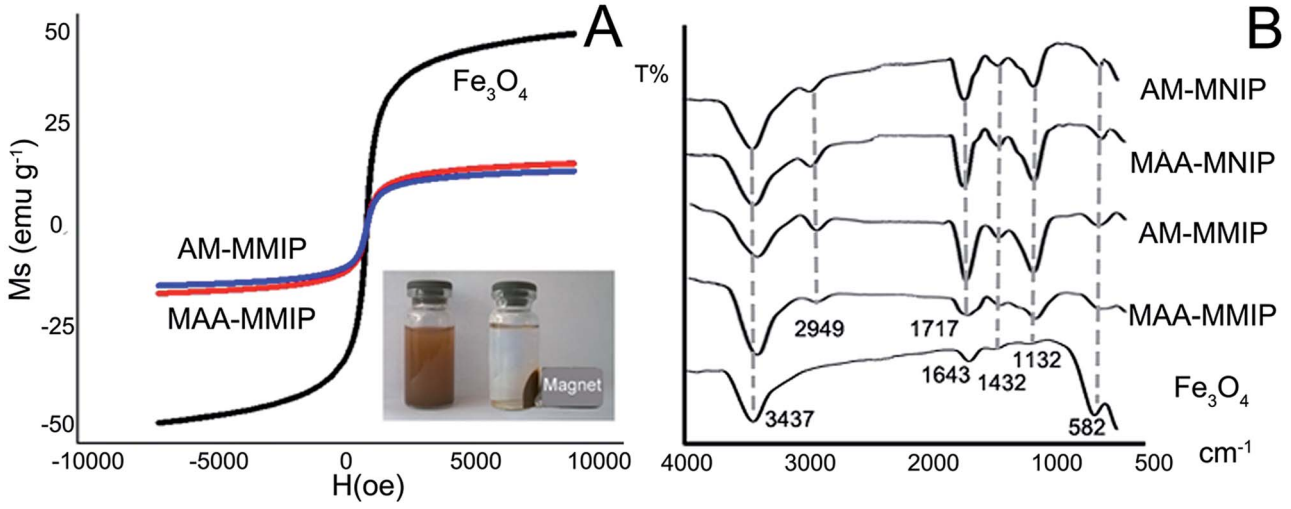

Fig. 3 Characterization of the nanomaterials: (A) VSM of Fe_3O_4, MAA-MMIP and AM-MMIP; (B) FT-IR spectra of 4 polymers and Fe_3O_4.

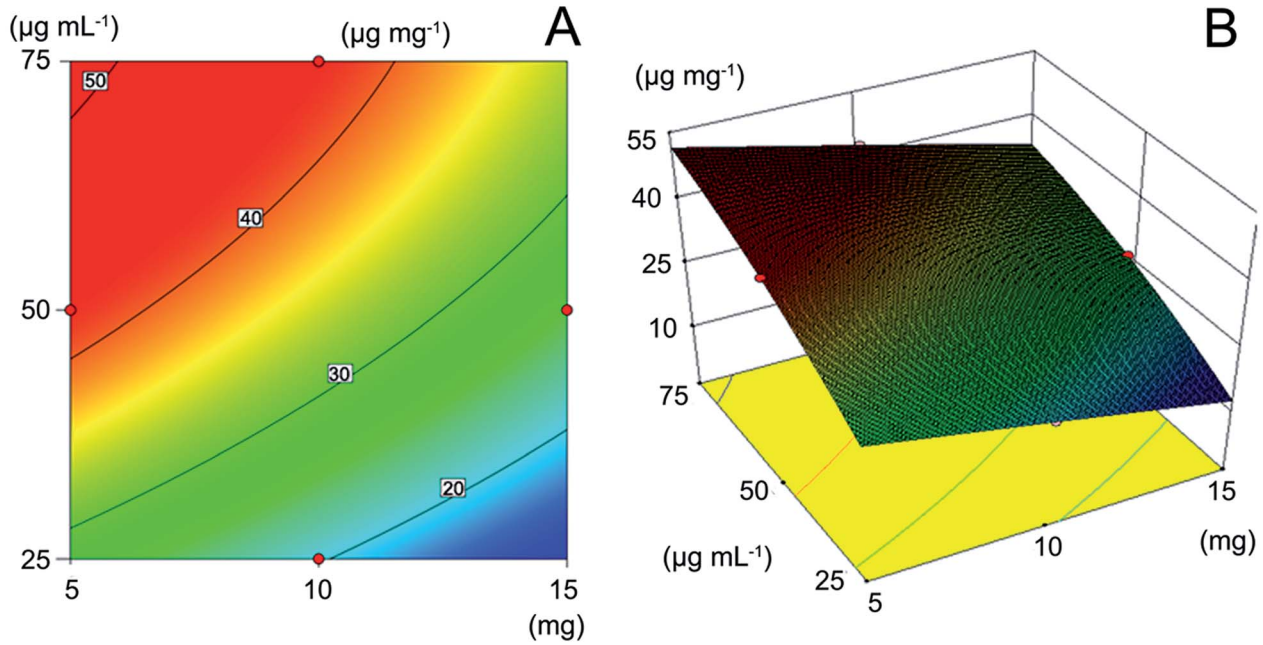

Fig. 4 Optimization of adsorption behavior with response surface methodology: (A) contour map of adsorption capacity; (B) response surface of three factors.

interaction term has been ignored. The equation of the model is described as:

$$\text{Adsorption capacity} = 30.22 - 8.84 \times A + 9.04 \times B - 3.80 \times C[1] + 0.12 \times C[2] - 0.66 \times AB - 1.44 \times AC[1] - 0.97 \times AC[2] - 1.54 \times BC[1] + 0.64 \times BC[2] - 0.14 \times A^2 - 2.63 \times B^2 \quad (5)$$

As showed in Fig. 4A, at the room temperature of 298 K which was close to the equilibrium temperature in molecular dynamics, the contour map represented the different combination of amount of polymer and concentration of the solution to get the adsorption capacity of 20, 30, 40, 50 μg mg^{-1} respectively. Fixed the amount of polymers, with the increase of solution concentration, the adsorption amount raised gradually due to the unbounding sites in the polymer. The increase of template would make the adsorption equilibrium move to the direction of larger adsorption capacity until the new equilibrium achieved. The adding of the polymer while the solution concentration remain unchanged, the adsorption amount decreased because of the intense competition owing to the increasing specific binding sites. The influence of reaction temperature with a small F value of 3054.15 in ANOVA is much less than other two factors showing the material is tolerant to high temperature (323 K). With the regression model obtained,

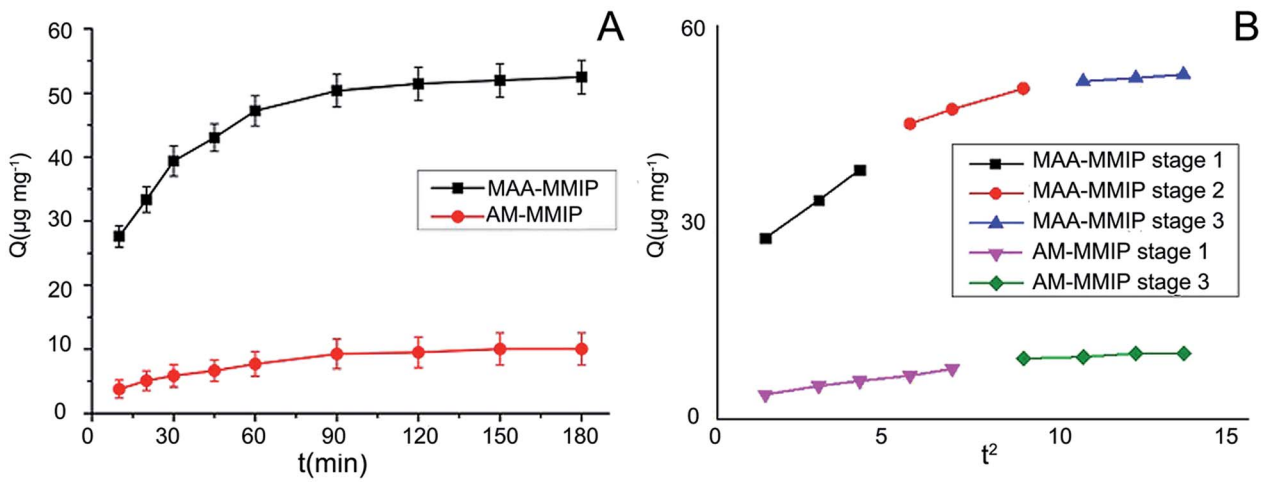

Fig. 5 (A) Adsorption kinetic curves for AML on MMIPs (AML: initial concentration: 75 μg mL^{-1}, volume: 10 mL; MMIPs amount: 5 mg; adsorption time: 0 min to 180 min); (B) plot of intra-particle diffusion model for adsorption of AML on MMIPs.

Table 3 Adsorption kinetic constants of models

	Pseudo-first-order kinetic model			Pseudo-second-order kinetic model		
Polymer	$Q_{e,cal}$ (μg mg^{-1})	K_1 (min)	R_1^2	$Q_{e,cal}$ (μg mg^{-1})	K_2 (g mg^{-1} min^{-1})	R_2^2
MAA-MMIP	31.31	0.0281	0.9850	56.17	0.0015	0.9995
AM-MMIP	10.03	0.0238	0.9789	11.64	0.0032	0.9954

the response surface was obtained (Fig. 4B) and the maximum adsorption capacity can be predicted under the given conditions.[32] The optimal adsorption condition is 4 mg MAA-MMIP in 4 mL drug solution of 75 μg mL^{-1} at 298 K, and the biggest adsorption capacity predicated was 51.66 μg mg^{-1}.

Binding property study

Adsorption kinetics. According to the RSM model obtained, adsorption kinetics study was carried out at the initial concentration of 75 μg mL^{-1}. Fig. 5A shows the adsorption amount of two polymers increase rapidly until 60 min and the adsorption equilibrium time are about 120 min. Pseudo-first-order kinetic model and pseudo-second-order kinetic model[33,34] were used to describe the kinetics of adsorption behavior in Table 3. The pseudo-first-order model is expressed as:

$$\ln(Q_e - Q_t) = \ln Q_e - K_1 t \quad (6)$$

The pseudo-second-order model is expressed as:

$$t/Q_t = t/Q_e + 1/(K_2 Q_e^2) \quad (7)$$

where Q_e and Q_t refer to adsorption amount (μg mg^{-1}) of the polymer at the equilibrium and time t (min). K_1 and K_2 are the constants of two kinetics models.

The intra-particle diffusion model[34] is expressed as:

$$Q_t = K_i t^{0.5} + C_i \quad (8)$$

where Q_t is the amount (μg mg^{-1}) of AML adsorbed at time t (min) and K_i is the rate constant. C_i is the intercept of the line, and represents the thickness of the boundary layer.

The larger correlation coefficients (R^2) indicate the adsorption behavior of AML on the two polymers followed pseudo-second-order kinetic model. It is chemisorption instead of physisorption in pseudo-first-order kinetic model.[35] Although the two polymers have formed specific binding sites for AML, it is about 5 times that the equilibrium adsorption capacity of MAA-MMIP compared to AM-MMIP as in computer simulation, more stable complex with 7 hydrogen bonds was formed between MAA and AML. The intra-particle diffusion model was proposed for further study on adsorption kinetics behavior. The result showed in Fig. 5B was a multi-linear plot and can be divided into 3 parts for MAA-MMIP but only 2 parts for AM-MMIP. At the first stage, there are plenty of non-binding sites both specific and non-specific sites on the surface of MAA-MMIP and AM-MMIP, so the adsorption amount increase quickly by external diffusion. The second stage for MAA-MMIP is internal diffusion. As showed in SEM graph, the surface of MAA-MMIP is much more uneven and full of caves, so the second stage is the interaction between AML and binding sites in the internal of MAA-MMIP but for AM-MMIP it directly came to final plateau. For AM-MMIP, obscure intra-particle diffusion stage points out that there are less specific binding sites in the polymer and it is the reason why MAA-MMIP has a larger adsorption amount and need a little more time for equilibrium than AM-MMIP.

Adsorption isotherm. With the concentration of AML varying from 25 to 75 μg mL^{-1}, the adsorption amount of two polymers were increasing as showed in Fig. 6. Langmuir and Freundlich isotherm model were used to study the static adsorption behavior. The Langmuir isotherm model[23] is described as:

$$C_e/Q_e = C_e/Q_m + 1/(Q_m K_L) \quad (9)$$

The Freundlich isotherm mode[36] is described as:

$$\ln Q_e = m \ln C_e + \ln K_F \quad (10)$$

where Q_e, C_e are equilibrium adsorption amount (μg mg^{-1}) and concentration (μg mL^{-1}), K_L and K_F are constants of two model. Q_m in Langmuir isotherm model is the maximum adsorption amount (μg mg^{-1}) predicted and m in Freundlich

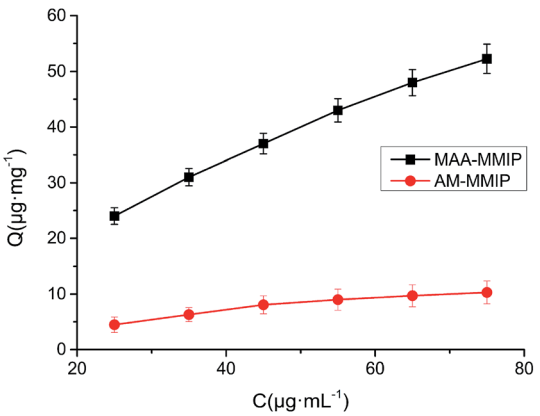

Fig. 6 Adsorption isotherm curves for AML on MMIPs (concentration of AML: 25–75 μg mL^{-1}, volume: 10 mL and MMIPs amount: 5 mg).

Table 4 Langmuir and Freundlich isotherm model parameters at 25 °C

	Langmuir isotherm model			Freundlich isotherm model		
Polymers	Q_m (μg mg^{-1})	K_L (mL μg^{-1})	R_1^2	K_F (μg mg^{-1})	m	R_2^2
MAA-MMIP	79.37	0.0354	0.9338	7.94	0.4995	0.9994
AM-MMIP	16.58	0.0197	0.9926	0.49	0.7145	0.9831

isotherm model is the surface heterogeneity index between 0 and 1.

The parameters of two isotherm model was listed in Table 4. The correlation coefficient of AM-MMIP is 0.9926 in Langmuir isotherm model which is used to describe the monolayer adsorption by homogeneous binding sites. The correlation coefficient of Freundlich isotherm model are more than 0.999 implying the isotherm behavior of MAA-MMIP belongs to the heterogeneous adsorption with multiple binding sites while Langmuir isotherm model is suitable for homogeneous system. The adsorption intensity (m) of MAA-MMIP and AM-MMIP is 0.4995 and 0.7145 indicating the great difference in the affinity of the binding sites. In addition the m value close to 1 means there are more homogeneous binding sites on the surface of the polymer, in other words there are much more non-specific binding sites in AM-MMIP reflecting the weaker interaction of functional monomer AM and template AML and the results were consistent with computer simulation.

The prediction of maximum adsorption amounts of MAA-MMIP by response surface quadratic model, pseudo-first-order model, pseudo-second-order model, Langmuir isotherm model and Freundlich isotherm model were listed in Table 5. Actual measured value is 53.77 μg mg^{-1} and the relative error of RSM is only 3.92% illustrating that RSM has a good accuracy in evaluation and prediction of adsorption properties for molecularly imprinted polymers.

Selectivity study

Three DHP-CCBs (NIM, NIF, and FEL) were selected as structural analogues for AML while PENI as non-structural analogues in selectivity study. As listed in Table 6, the imprinting factor of MAA-MMIP for AML and its structural analogues is more than 2 while only 1.02 for PENI reflecting that compared with MAA-MNIP proving that the polymer has formed specific cavities for this structure successfully. Moreover, α value of AML is slightly larger than other DHP-CCBs indicating that specific recognition cavities should be the most similar to the structure of template molecule AML. The results of AM-MMIP have not emerged the same trend for 5 drugs, so it was weak imprinting and lack of specific selectivity. The selectivity of the materials can be further illustrated by the differences in selectivity factor. The biggest β value was obtained from PENI by MAA-MMIP implying the polymer has greatest disparity in affinity between AML and PENI while there were only slight difference for other DHP-CCBs as the β value close to 1. All the results illustrated that MAA-MMIP had good specific selectivity.

Determination of AML in urine sample and validation of M-MISPE-UV method

M-MISPE-UV method was established, validated and applied in the pretreatment and detection of untreated urine samples spiked with different concentration of AML (5, 25, 75 μg mL^{-1}). The experiments were repeated for 3 times and the average recoveries were ranging from 94.7 to 101.6%. The linear range of the method for AML was 0.31–100 μg mL^{-1} with correlation coefficient 0.9991 and LOD (S/N = 3) was 0.12 μg mL^{-1}. The intraday repeatability (the experiments were repeated 6 times) and inter-day reproducibility, the relative standard deviations were from 2.05 to 3.61%. Compared with the other methods,[21,37–40] the simple method we proposed displays high, selectivity low interference and satisfactory recoveries without the use of the use of expensive instruments and complicated method.

Table 6 The selectivity parameters of the 4 materials

	Functional monomer	AML	PENI	NIM	NIF	FEL
Imprinting factor (α)	MAA	2.29	1.02	2.11	2.02	2.10
	AM	1.40	1.86	1.46	1.74	1.80
Selectivity factor (β)	MAA		2.24	1.08	1.13	1.09
	AM		1.23	1.57	1.32	1.27

Table 5 Comparison of each model and actual measured value for MAA-MMIP

	Actual measured value	Response surface quadratic model	Pseudo-first-order model	Pseudo-second-order model	Langmuir adsorption model	Freundlich adsorption model
Q_{max} (μg mg^{-1})	53.77	51.66	31.31	56.17	79.37	61.64
Correlation coefficient		0.9999	0.9950	0.9995	0.9938	0.9994
Relative error (%)		3.92	41.77	4.46	47.61	14.58

Conclusions

In this study, a simple, rapid and effective method for rational design of MIP has been established by combining flexible docking and molecular dynamics in computer simulation. Amlodipine magnetic molecularly imprinted polymer was prepared and response surface methodology as a powerful statistical method in the design of experiments and data processing has been applied in adsorption behavior study to acquire the comprehensive information in loading process and shorten the experimental time. Adsorption kinetics, isotherm and selectivity study of the polymer have been carried out to enhance the understanding of the adsorption mechanism. The MMIP with high selectivity and larger adsorption capacity is especially suitable for the enrichment and detection of amlodipine in urine sample as sorbent in magnetic solid phase extraction and provide a good practice for further application of M-MISPE in enrichment, separation and detection of drug in complex matrices.

Acknowledgements

This work was supported by the Open Project of Key Laboratory of Modern Toxicology of the Ministry of Education (Grant No. NMUMT201404), the Jiangsu Province Science Foundation for Youths (BK20130644) and the National Basic Science Personal Training Fund (No. J0630858).

Notes and references

1 H. F. Hawari, N. M. Samsudin, A. Y. M. Shakaff, Y. Wahab, U. Hashim, A. Zakaria, S. A. Ghani and M. N. Ahmad, *Sens. Actuators, B*, 2013, **187**, 434–444.
2 Y. Wen, L. Chen, J. Li, D. Liu and L. Chen, *TrAC, Trends Anal. Chem.*, 2014, **59**, 26–41.
3 T. S. Anirudhan and S. Sandeep, *Polym. Chem.*, 2011, **2**, 2052.
4 M. Behbahani, S. Bagheri, M. M. Amini, H. Sadeghi Abandansari, H. Reza Moazami and A. Bagheri, *J. Sep. Sci.*, 2014, **37**, 1610–1616.
5 X. Kong, R. Gao, X. He, L. Chen and Y. Zhang, *J. Chromatogr. A*, 2012, **1245**, 8–16.
6 M. Ding, X. Wu, L. Yuan, S. Wang, Y. Li, R. Wang, T. Wen, S. Du and X. Zhou, *J. Hazard. Mater.*, 2011, **191**, 177–183.
7 J. Yao, X. Li and W. Qin, *Anal. Chim. Acta*, 2008, **610**, 282–288.
8 I. A. Nicholls, H. S. Andersson, C. Charlton, H. Henschel, B. C. Karlsson, J. G. Karlsson, J. O'Mahony, A. M. Rosengren, K. J. Rosengren and S. Wikman, *Biosens. Bioelectron.*, 2009, **25**, 543–552.
9 M. Khodadadian and F. Ahmadi, *Talanta*, 2010, **81**, 1446–1453.
10 M. Tabandeh, S. Ghassamipour, H. Aqababa, M. Tabatabaei and M. Hasheminejad, *J. Chromatogr. B: Anal. Technol. Biomed. Life Sci.*, 2012, **898**, 24–31.
11 S. A. P. T. A. Sergeyeva, A. A. Brovko, E. A. Slinchenko, L. M. Sergeeva and A. V. El'skaya, *Anal. Chim. Acta*, 1999, **392**, 105–111.
12 C. Dong, X. Li, Z. Guo and J. Qi, *Anal. Chim. Acta*, 2009, **647**, 117–124.
13 M. B. Gholivand, M. Khodadadian and F. Ahmadi, *Anal. Chim. Acta*, 2010, **658**, 225–232.
14 P. Dramou, P. Zuo, H. He, L. A. Pham-Huy, W. Zou, D. Xiao, C. Pham-Huy and T. Ndorbor, *J. Mater. Chem. B*, 2013, **1**, 4099.
15 A. Azimi and M. Javanbakht, *Anal. Chim. Acta*, 2014, **812**, 184–190.
16 M. A. Bezerra, R. E. Santelli, E. P. Oliveira, L. S. Villar and L. A. Escaleira, *Talanta*, 2008, **76**, 965–977.
17 J. Wu, H. Zhang, N. Oturan, Y. Wang, L. Chen and M. A. Oturan, *Chemosphere*, 2012, **87**, 614–620.
18 C. Zhu and X. Liu, *Carbohydr. Polym.*, 2013, **92**, 1197–1202.
19 W. C. Ko, C. K. Chang, H. J. Wang, S. J. Wang and C. W. Hsieh, *Food Chem.*, 2015, **172**, 497–503.
20 M. J. Brown, G. T. McInnes, C. C. Papst, J. Zhang and T. M. MacDonald, *Lancet*, 2011, **377**, 312–320.
21 K. Luo, M. Liu, Q. Fu, E. Amut, A. Zeng and C. Chang, *J. Appl. Polym. Sci.*, 2012, **125**, 3524–3531.
22 S. L. Ferreira, R. E. Bruns, H. S. Ferreira, G. D. Matos, J. M. David, G. C. Brandao, E. G. da Silva, L. A. Portugal, P. S. dos Reis, A. S. Souza and W. N. dos Santos, *Anal. Chim. Acta*, 2007, **597**, 179–186.
23 L. Feng, L. Tan, H. Li, Z. Xu, G. Shen and Y. Tang, *Biosens. Bioelectron.*, 2015, **69**, 265–271.
24 F. Yanez, I. Chianella, S. A. Piletsky, A. Concheiro and C. Alvarez-Lorenzo, *Anal. Chim. Acta*, 2010, **659**, 178–185.
25 M. Plasencia, A. Pedersen, A. Arnaldsson, J.-C. Berthet and H. Jónsson, *Comput. Geosci.*, 2014, **65**, 110–117.
26 M. Azenha, B. Szefczyk, D. Loureiro, P. Kathirvel, M. N. Cordeiro and A. Fernando-Silva, *Langmuir*, 2011, **27**, 5062–5070.
27 J. Saloni, P. Lipkowski, S. S. R. Dasary, Y. Anjaneyulu, H. Yu and G. Hill, *Polymer*, 2011, **52**, 1206–1216.
28 P. Dramou, D. Xiao, H. He, T. Liu and W. Zou, *J. Sep. Sci.*, 2013, **36**, 898–906.
29 P. Dramou, P. Zuo, H. He, L. A. Pham-Huy, W. Zou, D. Xiao and C. Pham-Huy, *J. Chromatogr. A*, 2013, **1317**, 110–120.
30 L. Qiao, N. Gan, F. Hu, D. Wang, H. Lan, T. Li and H. Wang, *Microchim. Acta*, 2014, **181**, 1341–1351.
31 Y. Huang, Y. Yuan, Z. Zhou, J. Liang, Z. Chen and G. Li, *Appl. Surf. Sci.*, 2014, **292**, 378–386.
32 M. Meng, Y. Feng, M. Zhang, Y. Ji, J. Dai, Y. Liu, P. Yu and Y. Yan, *Chem. Eng. J.*, 2013, **231**, 132–145.
33 H. He, D. Xiao, J. He, H. Li, H. He, H. Dai and J. Peng, *Analyst*, 2014, **139**, 2459–2466.
34 X. Du, S. Lin, N. Gan, X. Chen, Y. Cao, T. Li and P. Zhan, *J. Sep. Sci.*, 2014, **37**, 1591–1600.
35 C. Gonzato, P. Pasetto, F. Bedoui, P.-E. Mazeran and K. Haupt, *Polym. Chem.*, 2014, **5**, 1313–1322.
36 L. Fan, Y. Zhang, X. Li, C. Luo, F. Lu and H. Qiu, *Colloids Surf., B*, 2012, **91**, 250–257.
37 G. Bahrami and S. Mirzaeei, *J. Pharm. Biomed. Anal.*, 2004, **36**, 163–168.
38 Z. H. Wei, L. N. Mu, Q. Q. Pang, Y. P. Huang and Z. S. Liu, *Electrophoresis*, 2012, **33**, 3021–3027.
39 M. Yacoub, A. A. Awwad, M. Alawi and T. Arafat, *J. Chromatogr. B: Anal. Technol. Biomed. Life Sci.*, 2013, **917–918**, 36–47.
40 P. Norouzi, V. K. Gupta, B. Larijani, S. Rasoolipour, F. Faridbod and M. R. Ganjali, *Talanta*, 2015, **131**, 577–584.